

Galaxy and Mass Assembly (GAMA): maximum-likelihood determination of the luminosity function and its evolution

J. Loveday,¹★ P. Norberg,² I. K. Baldry,³ J. Bland-Hawthorn,⁴ S. Brough,⁵
M. J. I. Brown,⁶ S. P. Driver,^{7,8} L. S. Kelvin⁹ and S. Phillipps¹⁰

¹*Astronomy Centre, University of Sussex, Falmer, Brighton BN1 9QH, UK*

²*Institute for Computational Cosmology, Department of Physics, Durham University, South Road, Durham DH1 3LE, UK*

³*Astrophysics Research Institute, Liverpool John Moores University, IC2, Liverpool Science Park, 146 Brownlow Hill, Liverpool L3 5RF, UK*

⁴*Sydney Institute for Astronomy, School of Physics, University of Sydney, NSW 2006, Australia*

⁵*Australian Astronomical Observatory, PO Box 915, North Ryde, NSW 1670, Australia*

⁶*School of Physics, Monash University, Clayton, Victoria 3800, Australia*

⁷*International Centre for Radio Astronomy Research (ICRAR), The University of Western Australia, 35 Stirling Highway, Crawley WA6009, Australia*

⁸*School of Physics & Astronomy, University of St Andrews, North Haugh, St Andrews KY16 9SS, UK*

⁹*Institut für Astro- und Teilchenphysik, Universität Innsbruck, Technikerstraße 25, A-6020 Innsbruck, Austria*

¹⁰*Astrophysics Group, HH Wills Physics Laboratory, University of Bristol, Tyndall Avenue, Bristol BS8 1TL, UK*

Accepted 2015 May 3. Received 2015 April 29; in original form 2015 February 21

ABSTRACT

We describe modifications to the joint stepwise maximum-likelihood method of Cole in order to simultaneously fit the Galaxy and Mass Assembly II galaxy luminosity function (LF), corrected for radial density variations, and its evolution with redshift. The whole sample is reasonably well fitted with luminosity (Q_e) and density (P_e) evolution parameters $Q_e, P_e \approx 1.0$, 1.0 but with significant degeneracies characterized by $Q_e \approx 1.4 - 0.4P_e$. Blue galaxies exhibit larger luminosity density evolution than red galaxies, as expected. We present the evolution-corrected r -band LF for the whole sample and for blue and red subsamples, using both Petrosian and Sérsic magnitudes. Petrosian magnitudes miss a substantial fraction of the flux of de Vaucouleurs profile galaxies: the Sérsic LF is substantially higher than the Petrosian LF at the bright end.

Key words: galaxies: evolution – galaxies: luminosity function, mass function – galaxies: statistics.

1 INTRODUCTION

The luminosity function (LF) is perhaps the most fundamental model-independent quantity that can be measured from a galaxy redshift survey. Reproducing the observed LF is the first requirement of a successful model of galaxy formation, and thus accurate measurements of the LF are important in constraining the physics of galaxy formation and evolution (e.g. Benson et al. 2003). In addition, accurate knowledge of the survey selection function (and hence LF) is required in order to determine the clustering of a flux-limited sample of galaxies (Cole 2011).

A standard $1/V_{\max}$ (Schmidt 1968) estimate of the LF is vulnerable to radial density variations within the sample. This vulnerability can be largely mitigated by multiplying the maximum volume in which each galaxy is visible, V_{\max} , by the integrated radial overdensity of a density-defining population (Baldry et al. 2006, 2012). Maximum-likelihood methods (Sandage, Tammann & Yahil 1979;

Efstathiou, Ellis & Peterson 1988), which assume that the luminosity and spatial dependence of the galaxy number density are separable, are, by construction, insensitive to density fluctuations. However, if the sample covers a significant redshift range, galaxy properties (such as luminosity) and number density are subject to systematic evolution with lookback time. All of the above methods must then either be applied to restricted redshift subsets of the data, or be modified to explicitly allow for evolution (e.g. Lin et al. 1999; Loveday et al. 2012).

Cole (2011) recently introduced a *joint stepwise maximum-likelihood* (JSWML) method, which jointly fits non-parametric estimates of the LF and the galaxy overdensity in radial bins, along with an evolution model. In this paper, we describe modifications made to the JSWML method in order to successfully apply it to the Galaxy and Mass Assembly (GAMA) survey (Driver et al. 2011). In the GAMA-II sample, L^* galaxies can be seen out to redshift $z \approx 0.35$, and so one has a reasonable redshift baseline over which to constrain luminosity and density evolution. Loveday et al. (2012) have previously investigated LF evolution in the GAMA-I sample, finding that at higher redshifts: all galaxy types were more

* E-mail: J.Loveday@sussex.ac.uk

luminous, blue galaxies had a higher comoving number density and red galaxies had a lower comoving number density. Here, we exploit the greater depth (0.4 mag) of GAMA-II versus GAMA-I, and use an estimator of galaxy evolution that does not assume a parametric form (e.g. a Schechter function) for the LF.

The paper is organized as follows. In Section 2, we describe the GAMA data used along with corrections made for its small level of incompleteness. Our adopted evolution model is described in Section 3 and the density-corrected V_{\max} method in Section 4. Methods for determining the evolution parameters are discussed in Section 5. We present tests of our methods using simulated data in Section 6 and apply them to GAMA data in Section 7. We briefly discuss our findings in Section 8 and conclude in Section 9.

Throughout, we assume a Hubble constant of $H_0 = 100 h \text{ km s}^{-1} \text{ Mpc}^{-1}$ and an $\Omega_M = 0.3$, $\Omega_\Lambda = 0.7$ cosmology in calculating distances, comoving volumes and luminosities.

2 GAMA-II DATA, K - AND COMPLETENESS CORRECTIONS

In 2013 April, the GAMA survey completed spectroscopic coverage of the three equatorial fields G09, G12 and G15. In GAMA-II, these fields were extended in area to cover $12^\circ \times 5^\circ$ each¹ and all galaxies were targeted to a Galactic-extinction-corrected Sloan Digital Sky Survey (SDSS; Abazajian et al. 2009) DR7 Petrosian r -band magnitude limit of $r = 19.8$ mag. In our analysis, we include all main-survey targets ($\text{SURVEY_CLASS} \geq 4$)² with reliable AUTOZ (Baldry et al. 2014) redshifts ($nQ \geq 3$) from TilingCatv43 (Baldry et al. 2010). Redshifts (from DistancesFramesv12) are corrected for local flow using the Tonry et al. (2000) attractor model as described by Baldry et al. (2012).

We calculate LFs using both Petrosian (1976) and Sérsic (1963) photometry, corrected for Galactic extinction using the dust maps of Schlegel, Finkbeiner & Davis (1998). We use single Sérsic model magnitudes truncated at 10 effective radii as fit by Kelvin et al. (2012). Kelvin et al. (2012) show that these recover essentially all of the flux for an $n = 1$ (exponential) profile, and about 96 per cent of the flux of an $n = 4$ (de Vaucouleurs) profile. SDSS Petrosian magnitudes, while also measuring almost all of the flux for exponential profiles, measure only about 82 per cent of the flux for de Vaucouleurs profiles (Blanton et al. 2001). Sérsic magnitudes are, however, more susceptible to contamination from nearby bright objects, which can cause them to be overestimated by several mag. We identify galaxies that may have contaminated photometry by searching for brighter stellar neighbours within a distance, up to a maximum of 5 arcmin, of twice the star’s isophotal radius (`isoA_r` in the SDSS `PhotoObj` table). Five per cent of GAMA targets are flagged in this way.

Fig. 1 shows a histogram of $\Delta m = r_{\text{Petro}} - r_{\text{Sersic}}$ for all GAMA-II main-survey targets (continuous blue histogram), and for targets without a nearby bright stellar neighbour (black dotted histogram). The majority (about 72 per cent) of excluded galaxies have positive Δm , i.e. are brighter in Sérsic than Petrosian magnitude. The dashed red histogram indicates targets without a nearby

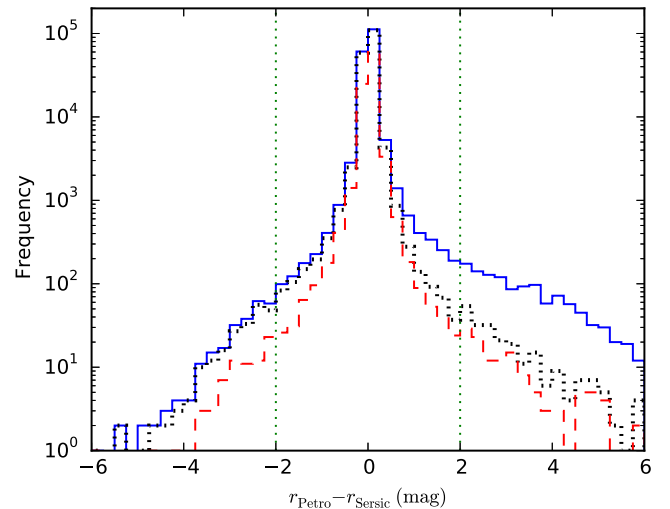


Figure 1. Histogram of the difference between Petrosian and Sérsic magnitudes for all GAMA-II main-survey targets (continuous blue histogram), and for targets without a nearby bright stellar neighbour, as defined in the text (black dotted histogram). The dashed red histogram indicates the subset of the latter targets classified as red. The vertical dotted lines denote the additional constraint $|r_{\text{Petro}} - r_{\text{Sersic}}| < 2.0$ mag required for galaxies to be assumed uncontaminated; only about 0.3 per cent of remaining targets lie beyond these limits.

bright stellar neighbour that are classified as red (as defined towards the end of this section). It is clear from this figure that uncontaminated red galaxies preferentially have brighter Sérsic than Petrosian magnitudes. This is as expected, assuming that they are bulge dominated, and hence have profiles with higher Sérsic index.

We exclude an additional 487 targets (0.3 per cent of the total) for which the r -band Sérsic and Petrosian magnitudes differ by more than 2 mag. This magnitude difference cut is somewhat arbitrary, but is designed to exclude galaxies with bright stellar neighbours that do not quite satisfy the above criterion (for instance if a galaxy lies on a star’s diffraction spike) or with bad sky background determination. It seems extremely unlikely that the Sérsic magnitude would recover more flux than this from an uncontaminated galaxy.

We have visually inspected these additional culled targets, for which $|\Delta m| = |r_{\text{Petro}} - r_{\text{Sersic}}| > 2$ mag, and placed them in one of the following categories: OK: no obvious problem; Deblend: large galaxy image likely to have been shredded by the SDSS deblending algorithm; FSC: nearby faint stellar companion (comparable to or fainter than target); BSC: nearby bright stellar companion (much brighter than target); Merger: nearby galaxy companion(s); Sky: bad sky background; NO: no object visible. The number of targets falling into each category, subdivided by whether Δm is positive (Sérsic flux is brighter) or negative (Petrosian flux is brighter) is given in Table 1. For the former sample, just over half of the cases of possibly overestimated Sérsic flux appear to be due to a nearby star which has more successfully been excluded from the Petrosian flux estimate. For the latter sample, the most common cause of underestimated Sérsic flux or overestimated Petrosian flux is likely due to deblending issues or a bad sky determination. We note that the presence of a nearby bright star should be totally uncorrelated with a galaxy’s intrinsic properties, and so excluding targets for this reason should not bias the sample in any way. A small bias could be caused by excluding the $\simeq 20$ per cent of inspected galaxies (about 0.06 per cent of total targets) for which the suspect photometry is caused by a neighbouring galaxy, since galaxies in crowded regions

¹ The RA, Dec. ranges of the three fields, all in degrees, are G09: 129.0–141.0, -2.0 to $+3.0$; G12: 174.0–186.0, -3.0 to $+2.0$; G15: 211.5–223.5, -2.0 to $+3.0$.

² Note that in this latest version of TilingCat, objects that failed visual inspection (`VIS_CLASS` = 2, 3 or 4) also have `SURVEY_CLASS` set to zero.

Table 1. Classification of the 487 GAMA targets without a bright stellar neighbour (as defined in the text) for which $\Delta m = r_{\text{Petro}} - r_{\text{Sersic}}$ lies outside the range $[-2, 2]$ mag. See text for meaning of first column.

Class	$\Delta m > 2$	$\Delta m < -2$
OK	12	42
Deblend	19	56
FSC	13	22
BSC	144	16
Merger	56	37
Sky	17	46
NO	7	0
Total	268	219

are expected to be more luminous than average. In cases when the Petrosian and Sérsic magnitudes differ by more than 2 mag, both magnitude estimates are suspect, and so it is debatable whether these objects should be GAMA targets at all. At worst, the effect of excluding targets with bright stellar neighbours or discrepant magnitudes (5.3 per cent of the entire GAMA-II sample) will be to bias the LF normalization low by up to 5 per cent.

After excluding GAMA main-survey targets with either an unreliable redshift (1.2 per cent) or suspect photometry (5.3 per cent), we are left with a sample of 173 527 galaxies in the redshift range $0.002 < z < 0.65$.

To determine K -corrections, we use `KCORRECT` v4.2 (Blanton & Roweis 2007) to fit spectral energy distributions to *ugriz* GAMA matched-aperture `SEXTRACTOR` (Bertin & Arnouts 1996) `AUTO` magnitudes taken from `ApMatchedCatv04` (Hill et al. 2011). As shown in appendix B of Taylor et al. (2011) and fig. 17 of Kelvin et al. (2012), SDSS model magnitudes, which have been recommended for calculating galaxy colours, e.g. Stoughton et al. (2002), are ill-behaved for galaxies of intermediate Sérsic index which are well fitted by neither pure exponential nor pure de Vaucouleurs profiles. GAMA matched-aperture magnitudes do not force a particular functional form on the galaxy profile and so provide more reliable colours for all galaxy types. In practice, we find that the choice of magnitude type used for K -corrections makes little difference to our LF estimates, with the Schechter fit parameters changing by less than 1σ . We use K -corrections to reference redshift $z_0 = 0.1$ in order to allow direct comparison with previous results (Loveday et al. 2012). For the three GAMA-II targets that are missing `AUTO` magnitudes, and for the 3.3 per cent of targets for which `KCORRECT` reports a χ^2 statistic of 10.0 or larger, implying a poor spectral energy distribution (SED) fit, we set the K -correction to the mean of the remaining sample. We have visually inspected 235 of these targets with poor-fitting SEDs. About 29 per cent are close to a bright star or are otherwise likely to suffer from poorly estimated sky background; about 22 per cent have one or more close neighbours and may thus suffer contaminated photometry; about 13 per cent show evidence of AGN activity. The remaining 35 per cent show no obvious reason for the SED fit to be poor, but it seems likely that many of these cases may be due to poor u -band photometry with underestimated errors.

While SDSS DR7 has improved photometric calibration over DR6 (used for selection of GAMA-I targets), it will suffer from the same surface-brightness-dependent selection effects as DR6, and so we assume the same *imaging completeness* C_{im} as shown in fig. 1

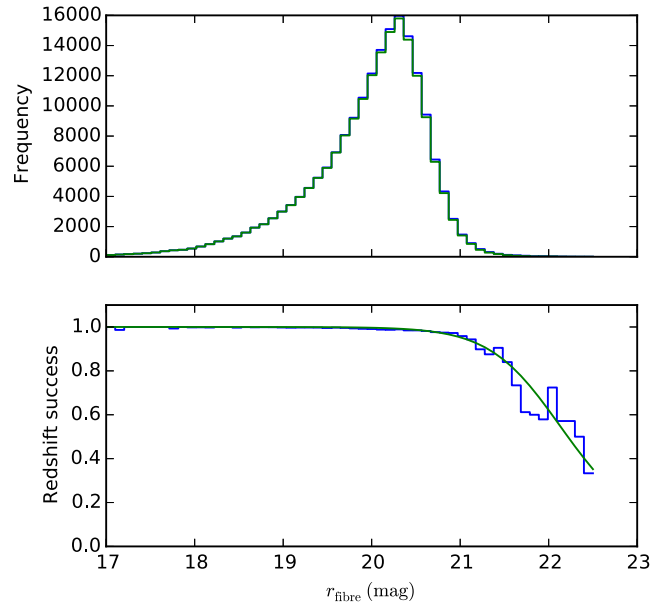


Figure 2. Redshift success rate as a function of r -band fibre magnitude. The top panel shows histograms of r_{fibre} for all observed galaxies in blue, and galaxies with a reliable redshift measurement ($n_Q > 2$) in green. Redshift success, the ratio of the latter to the former, is shown as a histogram in the lower panel, along with a best-fitting sigmoid-type function. The large fluctuations at faint magnitudes ($r_{\text{fibre}} > 21$) are simply due to small-number statistics: the success rate is the ratio of two small numbers.

of Loveday et al. (2012). In this paper, we only measure the r -band LF, and so assume that *target completeness* is 100 per cent. In fact, just 0.1 per cent of GAMA-II main targets with $r < 19.8$ mag lack a measured spectrum, with no systematic dependence on magnitude (Liske et al., submitted to MNRAS). Since GAMA-II uses a new, fully automated redshift measurement (Baldry et al. 2014), we have re-assessed *redshift success rate* for GAMA-II. Fig. 2 shows redshift success rate, defined as the fraction of observed galaxies with reliable ($n_Q \geq 3$) redshifts, as a function of r -band fibre magnitude. This success rate is well fitted by a modified sigmoid function

$$C_z = [1 + e^{a(r_{\text{fibre}} - b)}]^{-c} \quad (1)$$

with parameters $a = 2.55 \text{ mag}^{-1}$, $b = 22.42 \text{ mag}$ and $c = 2.24$. The extra parameter c (cf. Ellis & Bland-Hawthorn 2007; Loveday et al. 2012) is introduced to provide a more extended decline in C_z around $r_{\text{fibre}} \approx 20$ mag. Without it, the sigmoid function drops too sharply to faithfully follow the observed C_z .

Each galaxy is given a weight equal to the reciprocal of the product of imaging completeness and redshift success rate, $W_i = 1/(C_{\text{im}i}C_{z_i})$. A histogram of these weights is shown in Fig. 3. While the vast majority of galaxies (99.5 per cent) have $W_i < 2$, there is a tail of rare objects with weights as high as 100 or more. We have visually inspected the 157 objects with an assigned weight above 10.0. Of these, 38 per cent are close to a bright star or are otherwise likely to have a poorly determined sky background; another 38 per cent have nearby neighbouring galaxies, which might lead to a compromised surface-brightness estimate; 10 per cent are isolated and show no obvious visual indication of being of low surface brightness. That left just 14 per cent that appeared to be genuine low surface-brightness galaxies, potentially with half-light surface-brightness $\mu_{50,r} \gtrsim 24 \text{ mag arcsec}^{-2}$ and/or with fibre magnitude $r_{\text{fibre}} \gtrsim 22 \text{ mag}$. We therefore chose to set an upper limit cap of 5.0 on incompleteness weights, i.e. to set $W_i = \min(W_i, 5.0)$. This limit

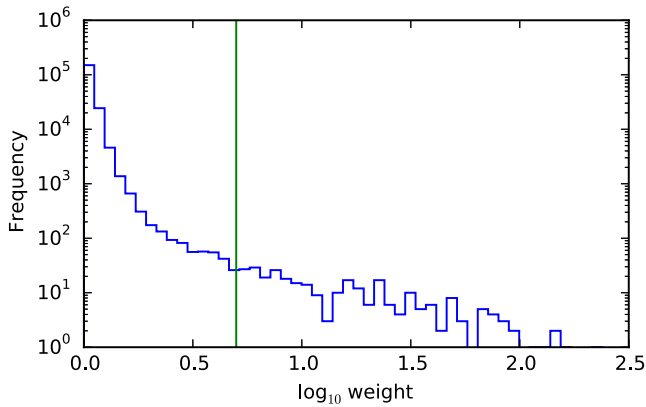


Figure 3. Histogram of completeness-correction weights for GAMA-II galaxies. Note that both axes use logarithmic binning. The vertical line corresponds to the applied upper limit weight cap of 5.0.

corresponds to the inverse redshift success rate for galaxies with the faintest fibre magnitudes (Fig. 2). While only 297 galaxies (0.16 per cent of the total) have $W_i > 5.0$, these galaxies are likely to lie at the extreme faint end of the LF, where there are few observed galaxies, and so spurious weights could potentially bias the LF faint end. The mean galaxy weights before and after applying this cap are 1.12 and 1.09, respectively.

The effect of applying this weight cap is to reduce the best-fitting value of the density evolution parameter P_e by about 40 per cent, with a corresponding increase in the best-fitting value of the luminosity evolution parameter Q_e . Best-fitting LF parameters change by less than 1σ .

When subdividing GAMA galaxies into blue and red subsamples, we use the colour cut of Loveday et al. (2012), namely

$$^{0.1}(g-r)_{\text{Kron}} = 0.15 - 0.03 \ ^{0.1}(M_r - 5 \log h). \quad (2)$$

A detailed investigation of colour bimodality in GAMA has recently been presented by Taylor et al. (2015). They utilize restframe and dust-corrected ($g-i$) colour, and argue that a probabilistic assignment of galaxies to ‘R’ and ‘B’ populations is preferable to a hard (and somewhat arbitrary) red/blue cut. They also emphasize that colour is not synonymous with morphological type, but rather provides a proxy for mean stellar age within a galaxy. Also, of course, a galaxy may appear red in uncorrected restframe colour due to dust extinction, rather than an old stellar population. In this paper, we stick with the simple colour cut of equation (2) for two reasons: (i) to allow direct comparison with the results of Loveday et al. (2012) and (ii) the Taylor et al. (2015) model of the colour–mass distribution has been tuned to a nearly volume-limited sample of galaxies at redshift $z < 0.12$ – the model parameters are likely to evolve at higher redshift.

Uncertainties in measured quantities, such as radial overdensity and the LF, are determined by jackknife resampling. We subdivide the GAMA-II area into nine $4^\circ \times 5^\circ$ regions, and then recalculate the quantity nine times, omitting each region in turn. For any quantity x , we may then determine its variance using

$$\text{Var}(x) = \frac{N-1}{N} \sum_{i=1}^N (x_i - \bar{x})^2, \quad (3)$$

where $N = 9$ is the number of jackknife regions, x_i is our estimate of x obtained when omitting region i and \bar{x} is the mean of the x_i . The numerator ($N - 1$) in the pre-factor allows for the fact that the jackknife estimates are not independent. Each jackknife region

contains an average of 19 281 galaxies for the full GAMA-II sample (i.e. without colour selection).

3 PARAMETRIZING THE EVOLUTION

We parametrize luminosity and density evolution over the redshift range $0.002 < z < 0.65$ using the parameters Q_e and P_e introduced by Lin et al. (1999). This model assumes that galaxy populations evolve linearly with redshift in absolute magnitude, parametrized by Q_e , and in log number density, parametrized by P_e . Specifically, the luminosity e -correction is given by $E(z) = Q_e(z - z_0)$, such that absolute magnitude M is determined from apparent magnitude m using

$$M = m - 5 \log_{10} d_L(z) - 25 - K(z; z_0) + Q_e(z - z_0), \quad (4)$$

where $d_L(z)$ is the luminosity distance (assuming the cosmological parameters specified in the Introduction) at redshift z and $K(z; z_0)$ is the K -correction, relative to a passband blueshifted by z_0 . Luminosity evolution is determined relative to the same redshift $z_0 = 0.1$ as the K -correction.

Evolution in number density $P(z)$ is parametrized as

$$P(z) = P(z_0) 10^{0.4 P_e (z - z_0)} = P(z = 0) 10^{0.4 P_e z}. \quad (5)$$

The motivation for this choice of parametrization is that if the shape of the LF does not evolve with redshift, that is it shifts only horizontally in absolute magnitude by Q_e , and vertically in log-density by P_e , then luminosity density ρ_L evolves as

$$\rho_L(z) = \rho_L(z_0) 10^{0.4(P_e + Q_e)(z - z_0)}. \quad (6)$$

While P_e and Q_e are strongly degenerate, and so poorly constrained individually, their sum $P_e + Q_e$ is well constrained (Lin et al. 1999; Loveday et al. 2012). We set further constraints on the linear combination of these parameters in Section 7.

4 DENSITY-CORRECTED V_{max} METHOD

In this section, we describe our technique for determining the LF using a maximum-likelihood, density-corrected V_{max} estimator, assuming that evolution is known. We will discuss how we determine the evolution parameters Q_e and P_e in Section 5. Our method is based on the JSWML method of Cole (2011), which jointly fits the LF and overdensities in radial bins of redshift caused by large-scale structure. Cole’s derivation starts with an expression for the *joint* probability of finding a galaxy at specified redshift and luminosity, and assumes that all galaxies have identical evolution- and K -corrections. We wish to allow for individual K - (and in the future e -) corrections, in which case it is easier to start with the *conditional* probability that an observed galaxy of luminosity L_i has a redshift z_i , assuming that the luminosity and spatial dependence of the galaxy number density are separable. This conditional probability is given by (Saunders et al. 1990):

$$p_i = \frac{\Delta(z_i) P(z_i) \frac{dV}{dz} \Big|_{z_i}}{\int_0^{z_{\text{max},i}} \Delta(z) P(z) \frac{dV}{dz} dz}. \quad (7)$$

Here, we have factored the mean density at redshift z , $\bar{n}(z) = \Delta(z) P(z)$, into a product of the galaxy overdensity³ $\Delta(z)$ due to large-scale structure times the steadily evolving density $P(z)$ from

³ Following Cole (2011), we use the term overdensity to mean a multiplicative relative density, so that $\Delta = 1$ corresponds to average density.

equation (5); dV/dz is the differential of the survey volume, and $z_{\max,i}$ is the maximum redshift at which galaxy i would still be visible, determined by the survey flux limit along with the galaxy's luminosity, K - and e -corrections.

Adopting binned estimates of the galaxy overdensity Δ , and weighting each galaxy by its incompleteness-correction weight, W_i , we obtain a log-likelihood

$$\ln \mathcal{L} = \sum_i W_i \left[\ln \sum_j \Delta_j P_j V_j D_{ij} - \ln \sum_j \Delta_j P_j V_j S_{ij} \right]. \quad (8)$$

Here V_j , P_j and Δ_j are the volume, density evolution and galaxy overdensity, respectively, in redshift bin j ; the function D_{ij} is a simple binning function, equal to unity if galaxy i lies in redshift bin j , zero otherwise, and S_{ij} is the fraction of redshift bin j in which galaxy i is visible. In the present analysis, we employ redshift bins of width $\Delta z = 0.01$. The maximum-likelihood solution for the overdensities Δ_j , given by $\partial \ln \mathcal{L} / \partial \Delta_j = 0$, may be obtained by iteration from:

$$\Delta_j = W_{\text{sum},j} \left[\sum_i \frac{W_i P_j V_j S_{ij}}{V_{\max,i}^{\text{dc}}} \right]^{-1}, \quad (9)$$

where $W_{\text{sum},j} = \sum_i W_i D_{ij}$ is the sum of galaxy weights in redshift bin j and $V_{\max,i}^{\text{dc}} = \sum_k \Delta_k P_k V_k S_{ik}$, the effective volume, corrected for evolution and fluctuations in radial density, within which galaxy i is visible.

The LF, unaffected by density fluctuations, may then be estimated by substituting $V_{\max,i}^{\text{dc}}$ for the usual expression for V_{\max} :

$$\phi_l^{\text{bin}} = \sum_i \frac{W_i D_{il}}{V_{\max,i}^{\text{dc}}}, \quad (10)$$

where $D_{il} = 1$ if galaxy i is in luminosity bin l , zero otherwise. Cole (2011) shows that this expression may be derived via maximum likelihood, at least in the case of identical e - and K -corrections.

Cole also discusses an extension to this method whereby parameter(s) describing the density evolution $P(z)$ may be determined simultaneously with the overdensities Δ_j by adding prior constraints on the values of Δ_j using the known clustering of galaxies. However, for our choice of density evolution parametrization (equation 5), the derivative in Cole equation (25) no longer depends explicitly on the evolution parameter, leading to a lack of convergence. We therefore prefer to search over both luminosity and density evolution parameters, as described in the next section.

A stepwise estimate of the LF, as given by equation (10), is not constrained to vary smoothly from bin to bin. Furthermore, at very low and high luminosity there may be bins containing no galaxies, resulting in an ill-defined log-likelihood (see equation 12 below). This problem is exacerbated when exploring possible values of the luminosity evolution parameter Q_e , as galaxies will then shift from bin to bin as Q_e is varied, resulting in unphysical sharp jumps in likelihood. To overcome these problems, we employ a Gaussian-smoothed estimate of the LF:

$$\phi_l^{\text{GS}} = \sum_i \frac{W_i}{V_{\max,i}^{\text{dc}}} G \left(\frac{M_i - M_l}{b} \right). \quad (11)$$

Here, the smoothing kernel G is a standard Gaussian, b is the smoothing bandwidth, M_i is the (K - and e -corrected) absolute magnitude of galaxy i and M_l is the absolute magnitude at the centre of bin l . In order not to underestimate the extreme faint end of the LF, it is important to apply boundary conditions to ϕ^{GS} corresponding to the chosen range of absolute magnitudes. We do this using the

default renormalization method and bandwidth choice of the python module `PYQT_FIT.KDE`.⁴ ϕ^{GS} does not, of course, correspond to the true galaxy LF, but rather to the LF convolved with a Gaussian of standard deviation b . Therefore, when plotting the LF and fitting a Schechter function, we use the standard binned LF ϕ^{bin} rather than ϕ^{GS} .

5 DETERMINING EVOLUTION PARAMETERS

In Cole's original derivation of this method, one maximizes a posterior likelihood (Cole equation 38)⁵ over the luminosity evolution parameter Q_e (Cole calls this parameter u). When applying this method to GAMA data, we found that the estimated value of Q_e diverged, unless one places an extremely tight prior on its value.⁶ Our problem was traced to the fact that varying Q_e changes all of the inferred absolute magnitudes (as well as visibility limits) for each galaxy. Choosing fixed absolute magnitude limits within which to determine the LF thus results in a change of sample size as Q_e varies, leading to likelihoods that cannot be directly compared. Even if one includes the term on the second line of Cole equation (36), which yields $-N_{\text{tot}} \ln \hat{N}_{\text{tot}}$ in the case of identical K - and e -corrections, the estimate of Q_e still diverges as galaxies shift systematically brighter or fainter as Q_e decreases or increases. We therefore consider two alternative methods to optimize the evolution parameters.

5.1 Mean probability

Our first solution is to consider not the product of the probabilities of observing each galaxy, but instead the *geometric mean* of the probabilities, which does not vary systematically with sample size N . Our pseudo-log-likelihood $\ln \mathcal{P}$ is then given by (Cole equation 36)

$$\begin{aligned} \ln \mathcal{P} = & \frac{1}{N} \sum_j W_{\text{sum},j} \ln(V_j P_j \Delta_j) + \frac{1}{N} \sum_l W_{\text{sum},l} \ln \phi_l^{\text{GS}} \\ & - \frac{1}{N} \sum_i W_i \ln \sum_j V_j P_j \Delta_j \sum_l \phi_l^{\text{GS}} S(L_{\min,i,j} | L_l) \\ & - \sum_j \frac{(\Delta_j - 1)^2}{2\sigma_{\Delta_j}^2} - \frac{(Q_e - Q_0)^2}{2\sigma_{Q_e}^2} - \frac{(P_e - P_0)^2}{2\sigma_{P_e}^2}, \quad (12) \end{aligned}$$

where $W_{\text{sum},j}$ is the sum of galaxy weights in redshift bin j , $W_{\text{sum},l}$ is the sum of galaxy weights in luminosity bin l and $S(L_{\min,i,j} | L_l)$ is the fraction of luminosity bin l for which galaxy i at redshift z_j would be visible. The term on the second line is a constant in the case of identical K - and e -corrections; with identical e -corrections but independent K -corrections we find that including this term makes a negligible difference to the maximum-likelihood solution. The terms on the third line are priors on the radial overdensities Δ_j and

⁴ <https://pypi.python.org/pypi/PyQt-Fit>.

⁵ Note that Cole equations (36)–(38) are missing factors of P_p , such that each occurrence of V_p should read $V_p P_p$.

⁶ We believe that the reason that the test described in section 5 of Cole (2011) was successful was due to (i) placing a very tight prior ($\sigma = 0.05$) on the density evolution parameter and (ii) simulating a very deep galaxy survey (extending to magnitude $r < 24$ and redshift $z < 1.4$). Both of these factors minimize the degeneracy between luminosity and density evolution, and hence aid convergence. The GAMA-II sample is significantly shallower ($r < 19.8$, $z < 0.65$), and we do not wish to place tight prior constraints on either of the evolution parameters.

the evolution parameters P_e and Q_e . The priors on Δ_j are essential, as these values are completely degenerate with the density evolution parameter P_e . As discussed by Cole, the expected variance in Δ_j is given by

$$\langle \sigma_{\Delta_j}^2 \rangle = \frac{1 + 4\pi \hat{n}_j J_3}{\hat{n}_j V_j}, \quad (13)$$

with \hat{n}_j the predicted density and V_j the volume of redshift bin j . The factor $J_3 = \int r^2 \xi(r) dr \approx 2000 h^{-3} \text{Mpc}^3$ accounts for the fact that because galaxies are clustered, they tend to come in clumps of $4\pi \hat{n}_j J_3$ galaxies at a time (Peebles 1980). We find, however, that much more reliable estimates of $\sigma_{\Delta_j}^2$ are obtained from jackknife sampling – see Fig. 6 below. This is particularly true in the higher redshift bins, where one is sampling the clustering of the most luminous galaxies, and where adopting a universal value for J_3 underestimates the actual density fluctuations observed between jackknife samples. The priors on P_e and Q_e are optional, and may help convergence in some cases. We adopt broad priors of $(Q_0, \sigma_{Q_e}^2) = (1, 1)$ and $(P_0, \sigma_{P_e}^2) = (2, 1)$. These values were chosen to be consistent with the findings of Loveday et al. (2012) while still allowing some freedom for the optimum values to change under the present analysis.

5.2 LF–redshift χ^2

Our second method compares LFs estimated in two or more redshift ranges: if the evolution and density variations are correctly modelled, then the LFs should be in good agreement; if evolution parameters are poorly estimated, then one would expect poor agreement. We then minimize the χ^2 ($\equiv -2 \ln \mathcal{L}$) given by

$$\chi^2 = \sum_{j,k>j} \sum_l \frac{(\phi_l^j - \phi_l^k)^2}{\text{Var}(\phi_l^j) + \text{Var}(\phi_l^k)} + \sum_j \frac{(\Delta_j - 1)^2}{\sigma_{\Delta_j}^2}, \quad (14)$$

where ϕ_l^j is the Gaussian-smoothed LF in magnitude bin l for the broad redshift range j , and $\text{Var}(\phi_l^j)$ is the corresponding variance, determined by jackknife resampling. We restrict the sum over magnitude bins l to those bins which are complete given the redshift limits (see section 3.3 of Loveday et al. 2012) and which include at least 10 galaxies for all values of Q_e between specified limits. In practice, we have found best results are achieved using just two redshift ranges, split near the median redshift of the sample, $\bar{z} \approx 0.2$, so that the ‘knee’ region of the LF around L^* is well-sampled by both, and hence the degeneracies between luminosity and density evolution are minimized. If one chooses three or more redshift ranges, there will be very little luminosity coverage in common to the lowest and highest ranges, and so one does not really gain much information in doing so. Again, it is essential to place a prior on the overdensities (final sum in equation 14, with $\sigma_{\Delta_j}^2$ also determined from jackknife resampling) to remove the degeneracy with density evolution. This method places no priors on the values for the evolution parameters.

5.3 Finding optimum evolution parameters

We first evaluate χ^2 values, using each of the above methods, on a rectangular grid of (P_e, Q_e) , thus allowing one to visualize the correlations between the evolution parameters. The grid point with the smallest χ^2 value is then used as a starting point for a downhill simplex minimization to refine the parameter values corresponding to minimum χ^2 .

In order to quantify the degeneracy between evolution parameters, we slice the χ^2 grid in bins of P_e . For each slice, we fit a quadratic function to $\chi^2(Q_e)$ using the five (Q_e, χ^2) values closest to the point of minimum χ^2 in that slice. Using this quadratic fit, we locate the point $Q_{e,\chi^2_{\min}}$ of minimum χ^2 and its 1σ range, i.e. the range of Q_e values where χ^2 increases by unity from the minimum. We find both for simulations and for real data that the $Q_{e,\chi^2_{\min}} - P_e$ relation is very well fitted by a straight line, and so we perform a linear least-squares fit to $(P_e, Q_{e,\chi^2_{\min}})$ to obtain the relation $Q_e = mP_e + c$ which minimizes χ^2 .

6 TESTS USING SIMULATED DATA

6.1 The simulations

In this section, we test our implementation of the JSWML estimator using simulated data, following the procedure outlined in section 5 of Cole (2011).

We start by choosing a model LF with Schechter (1976) and evolution parameters close to those obtained from the GAMA-I survey by Loveday et al. (2012) and as given in Table 2. We then randomly generate redshifts with a uniform density in comoving coordinates, modulated by our assumed density evolution (equation 5), over the range $0.002 < z < 0.65$. Absolute magnitudes are selected randomly according to our assumed Schechter function from the range $-24 < M < -12$. From each absolute magnitude, we subtract $Q_e(z - 0.1)$ to model luminosity evolution. We then assign apparent magnitudes r using K -correction coefficients selected randomly from the GAMA-II data and reject simulated galaxies fainter than $r = 19.8$. This process is repeated until sufficient random galaxies have been generated to give the required number density,

$$N_{\text{sim}} = \int_{z_{\min}}^{z_{\max}} \int_{L_{\min}(z, m_{\min})}^{L_{\max}(z, m_{\max})} \phi(L, z) dL \frac{dV}{dz} dz, \quad (15)$$

within a volume corresponding to that of the three GAMA-II fields, viz $3 \times 5^\circ \times 12^\circ = 180 \text{ deg}^2$.

In order to simulate the effects of galaxy clustering, we split the simulated volume into 65 redshift shells p of equal thickness $\Delta z \approx 0.01$ and with volume V_j . For each shell, we generate a random density perturbation δ_j drawn from a Gaussian with zero mean and variance $4\pi J_3 / V_j$, with $4\pi J_3 = 30,000 h^{-3} \text{Mpc}^3$. We then randomly resample $N'_j = (1 + \delta_j)N_j$ of the original N_j simulated galaxies in each shell p , thus producing fluctuations consistent with the assumed value of J_3 .

Imaging completeness and redshift success are modelled by generating surface brightnesses and fibre magnitude for each simulated galaxy according to the relations observed in GAMA-I data, see

Table 2. Mean and standard deviation of the evolution and Schechter parameters recovered from 10 simulated GAMA catalogues. Parameters m and c quantify the linear relation $Q_e = mP_e + c$ which minimizes χ^2 .

Parameter	True	Mean prob	LF–redshift χ^2
Q_e	0.7	0.68 ± 0.23	0.61 ± 0.14
P_e	1.8	1.71 ± 0.67	1.88 ± 0.54
$\text{Cov}(Q_e, P_e)$		-0.16	-0.08
m		-0.37 ± 0.01	-0.33 ± 0.01
c		1.31 ± 0.09	1.24 ± 0.07
α	-1.23	-1.23 ± 0.02	-1.23 ± 0.01
$M^* - 5 \log h$	-20.70	-20.72 ± 0.06	-20.74 ± 0.03
$\log(\phi^*/h^3 \text{Mpc}^{-3})$	-2.00	-2.10 ± 0.09	-2.12 ± 0.07

appendix A1 of Loveday et al. (2012). Imaging completeness C_{im} is then determined from fig. 1 of Loveday et al. (2012) and redshift success C_z from equation (1). Simulated galaxies are then chosen randomly with probability equal to $C_{\text{im}}C_z$ and assigned a weight $W_i = 1/(C_{\text{im}}C_z)$ to compensate for those simulated galaxies omitted from the sample.

This procedure is repeated to generate 10 independent mock catalogues, each containing around 180 000 galaxies. These mock catalogues are run through the JSWML estimator, with evolution parameters being determined using both methods discussed in the previous section. Since the mock galaxies are clustered only in redshift shells and not in projected coordinates on the sky, we determine the expected variance in overdensity using equation (13) rather than jackknife resampling. We employ 65 redshift shells out to $z = 0.65$ and calculate the LF in bins of $\Delta M = 0.25$ mag over the range $-23 < M < -15$ mag.

6.2 Simulation results

The mean and standard deviation of each recovered parameter, and the covariance between evolution parameters, are given in Table 2. We see that the input evolution and LF parameters are recovered within about one standard deviation for both methods.

Fig. 4 shows 95 per cent confidence limits on the evolution parameters measured from each of the simulations. We see that the error contours are significantly smaller using the LF-redshift χ^2 method compared with the mean probability method. However, this

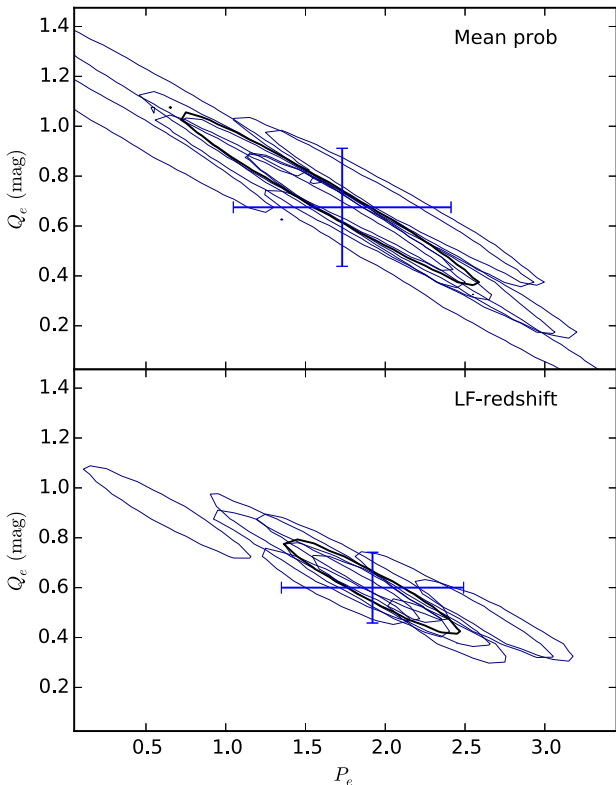


Figure 4. 95 per cent confidence limits on evolution parameters determined from 10 simulated data sets (light contours) and their average (heavy contour) determined using (top) mean probability (equation 12) and (bottom) LF-redshift χ^2 (equation 14). The error bars show the mean and standard deviation of the (P_e, Q_e) parameters from each simulation which yield minimum χ^2 . The input evolution parameters for these simulations were $P_e = 1.8$, $Q_e = 0.7$.

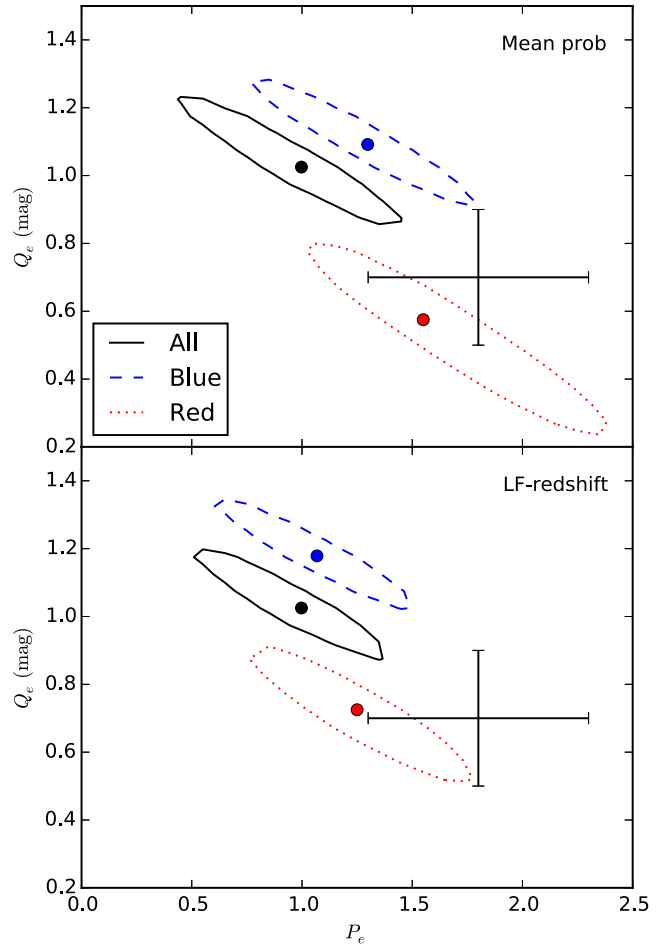


Figure 5. 95 per cent confidence limits on GAMA-II evolution parameters for all, blue and red galaxies as labelled. The upper panel shows the limits obtained using mean probability (equation 12); the lower panel shows results using LF-redshift χ^2 (equation 14). The large dots indicate the location of minimum χ^2 . The large error bars show the evolution parameters and 68 per cent confidence limits estimated for the combined GAMA-I sample in the r band by Loveday et al. (2012, Q_{par} and P_{par} from table 5).

test is idealized, in that our choice of evolution parametrization is identical in the simulations and in the analysis,⁷ and so we will apply both methods of constraining evolution parameters to the GAMA data in the following section. Note that the simulations have no inbuilt covariance between evolution parameters: they all use identical values of P_e and Q_e . The degeneracies (as quantified by $\text{Cov}(Q_e, P_e)$ and the parameters m and c in Table 2) arise as a result of the fitting process. For an LF described by an unbroken power law, the degeneracy between P_e and Q_e would be total, i.e. evolution in luminosity and density would be indistinguishable.

7 RESULTS FROM GAMA

7.1 Evolution

Fig. 5 shows 95 per cent confidence limits on the evolution parameters P_e , Q_e determined using equations (12) and (14) for the full GAMA-II sample and for blue and red galaxies separately. We see

⁷ We are performing a self-consistency test. It is unlikely that real galaxy populations evolve exactly according to our parametrization.

Table 3. Best-fitting evolution parameters for GAMA-II galaxy samples obtained using both mean probability and LF-redshift methods. Parameters m and c quantify the linear relation $Q_e = mP_e + c$. For the LF-redshift method only, χ_v^2 is the reduced χ^2 from equation (14); The uncertainties quoted on Q_e and P_e come from the bounding box containing the 1σ likelihood contour; the uncertainty on $P_e + Q_e$ is given by the distance from the point of minimum χ^2 to the 1σ likelihood contour along the direction $P_e = Q_e$.

Sample	Q_e	P_e	$Q_e + P_e$	m	c	χ_v^2
Mean probability						
All	1.03 ± 0.10	1.00 ± 0.25	2.02 ± 0.05	-0.36	1.38	...
Blue	1.09 ± 0.10	1.30 ± 0.25	2.39 ± 0.04	-0.35	1.55	...
Red	0.58 ± 0.18	1.55 ± 0.40	2.12 ± 0.08	-0.38	1.17	...
LF-redshift						
All	1.03 ± 0.07	1.00 ± 0.20	2.02 ± 0.05	-0.35	1.37	3.76
Blue	1.18 ± 0.05	1.07 ± 0.15	2.25 ± 0.04	-0.34	1.55	3.46
Red	0.73 ± 0.10	1.25 ± 0.25	1.98 ± 0.06	-0.36	1.16	3.35

Table 4. Best-fitting r -band LF parameters for GAMA-II galaxy samples obtained using both mean probability and LF-redshift methods. For the latter method, we show LF parameters obtained using both Petrosian and Sérsic magnitudes. χ_v^2 is the reduced χ^2 from least-squares Schechter function fits to the LF estimates; none of the LFs is well fitted in detail by a Schechter function, particularly at the bright end. The uncertainties quoted on the LF parameters come from jackknife sampling, but do not explicitly include the large degeneracies between them.

Sample	α	$M^* - 5\log h$	$\log \phi^* / h^3 \text{ Mpc}^{-3}$	χ_v^2
Mean probability Petrosian				
All	-1.26 ± 0.07	-20.71 ± 0.05	-2.02 ± 0.04	2.33
Blue	-1.38 ± 0.06	-20.36 ± 0.05	-2.27 ± 0.05	0.96
Red	-0.79 ± 0.11	-20.68 ± 0.06	-2.23 ± 0.05	3.48
LF-redshift Petrosian				
All	-1.26 ± 0.07	-20.71 ± 0.05	-2.02 ± 0.04	2.33
Blue	-1.37 ± 0.06	-20.35 ± 0.05	-2.24 ± 0.05	1.01
Red	-0.77 ± 0.11	-20.64 ± 0.05	-2.20 ± 0.04	3.01
LF-redshift Sérsic				
All	-1.30 ± 0.06	-20.88 ± 0.06	-2.13 ± 0.04	2.96
Blue	-1.39 ± 0.07	-20.40 ± 0.06	-2.27 ± 0.05	1.03
Red	-0.79 ± 0.12	-20.72 ± 0.07	-2.21 ± 0.05	4.91

that the confidence limits obtained with the two different methods largely overlap, although there are small differences between them. Best-fitting evolution parameters are given in Table 3. The difference in LFs obtained using evolution parameters determined with the two different methods is negligible (much less than the 1σ random errors; see Table 4). This illustrates the robustness of the LF estimate to the individual values assumed for P_e and Q_e : as long as their joint estimate is reasonable, e.g. they lie within the 95 per cent likelihood contours of Fig. 5, then overestimating one evolution parameter (e.g. P_e) is largely compensated for by underestimating the other (e.g. Q_e).

The differences in density evolution (P_e) for red and blue galaxies are not significant. Blue galaxies do however exhibit significantly stronger evolution in luminosity (Q_e) and in luminosity density ($Q_e + P_e$) than red galaxies, at the $\sim 5\sigma$ level.

The differences between red and blue galaxies agree qualitatively with those of Loveday et al. (2012), although in the present analysis we no longer see any evidence for negative density evolution for red galaxies. The three samples show very similar degeneracies in

(P_e, Q_e) parameter space. The errors on P_e and Q_e in Table 3 are the formal errors obtained by holding one parameter fixed and varying the other until χ^2 increases by one. Given the scatter in 95 per cent confidence limits between simulations shown in Fig. 4, more realistic errors, and their covariance, may be obtained from Table 2.

Since the exact values assumed for the evolution parameters have such a small effect on the LF parameters, see Table 4 below, for the remainder of this paper we assume evolution parameters found from the LF-redshift method in the lower half of Table 3.

7.2 Radial overdensities

Radial overdensities are shown in Fig. 6. While our evolution model is performing well, insofar as $\Delta(z)$ oscillates about unity, for redshifts $z \lesssim 0.5$, beyond this limit the overdensities are systematically high. This effect is almost entirely due to red galaxies, suggesting that luminosity and/or density evolution increases sharply at $z \approx 0.5$ for these galaxies compared with our model (section 3). It seems unlikely that incompleteness corrections could cause this, as there is no noticeable increase in weights beyond $z = 0.5$. Only 0.8 per cent of GAMA-II main-survey galaxies lie beyond $z = 0.5$, too few to constrain a more complicated evolution model, or to look for a large overdensity at these redshifts, see Fig. 7.

Below redshifts $z = 0.5$, we see the same features in radial overdensity in all three samples, although the fluctuations, as expected, are slightly more pronounced in the red galaxy sample. Note that the error bands given by equation (13) (shaded regions in Fig. 6) are significantly larger/smaller than the jackknife errors at low/high redshift. There are two reasons for this: (i) the low-redshift bins sample too small a volume for the J_3 integral to have converged and (ii) the low-/high-redshift bins are dominated by faint/luminous galaxies, with weaker/stronger clustering than the average defined by the assumed value of J_3 . This is why we use jackknife errors rather than the predicted variance in determining $\sigma_{\delta_j}^2$. We have tried halving the number of redshift bins to 32, verifying that the fitted parameters are insensitive to the redshift binning, with parameters changing by less than 1σ when the redshift bin size is doubled from $\Delta z = 0.01$ to $\Delta z = 0.02$.

7.3 LFs

Petrosian and Sérsic r -band LFs are shown in Fig. 8. Surface-brightness and redshift incompleteness have been taken into

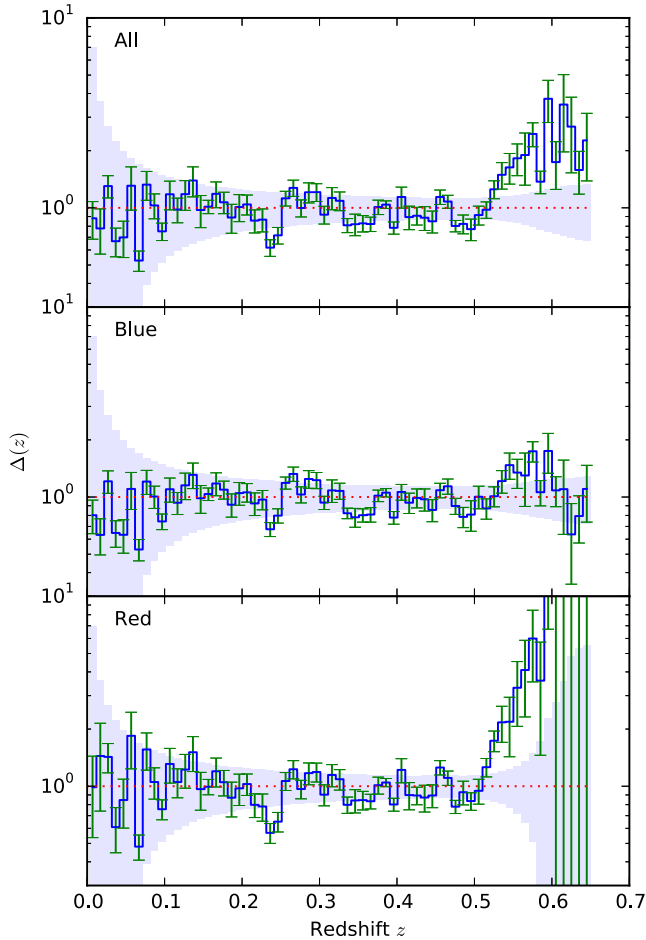


Figure 6. Radial overdensities determined from GAMA-II using the entire sample and blue and red subsets as labelled, assuming evolution parameters as given in the lower half of Table 3. The error bars show uncertainties estimated from jackknife sampling and the shaded regions centred on $\Delta = 1$ show the expected variance from equation (13).

account by appropriately weighting each galaxy (up to a maximum weight of 5.0, Section 2). We have fit a Schechter function to each binned LF using least squares; the fit parameters are tabulated in Table 4. Note that the Schechter fit for red galaxies underestimates the faint end of the LF (as well as the bright end – see below). It is likely that the faint-end upturn for red galaxies is at least partly due to the inclusion of dusty spirals in this sample; the luminosity and stellar mass functions of E–Sa galaxies of Kelvin et al. (2014a,b) show no indication of a faint-end or low-mass upturn. Fig. 5 of Kelvin et al. (2014b) shows that while very few galaxies with elliptical morphology are blue ($(g - i)_0 \lesssim 0.6$), the converse is not true: a substantial number of galaxies with spiral morphology are red ($(g - i)_0 \gtrsim 0.8$). Any upturn in the luminosity or mass function of spheroidal galaxies is more likely to be due to the presence of the so-called little blue spheroids (Kelvin et al. 2014b, fig. A1). Finally, we note that Taylor et al. (2015) have shown that the shape of the low-mass end of the stellar mass function of red galaxies is sensitive to how ‘red’ is defined. A low-mass upturn is seen when using the definition of Peng et al. (2010), but not when using those of Bell et al. (2003) and Baldry et al. (2004).

The red galaxy LF, and that for the combined sample, shows a bright-end excess: there are significantly more high-luminosity ($M_r - 5 \log h < -23$ mag) galaxies than predicted by the Schechter

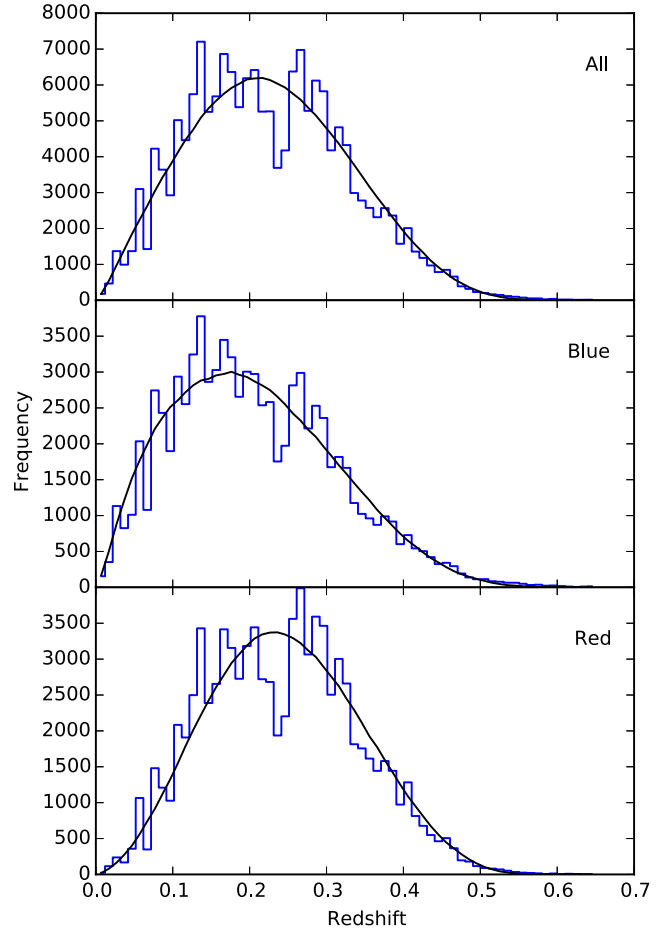


Figure 7. Redshift histograms for the whole GAMA-II sample and for blue and red galaxies separately. The curves in each panel give the predicted redshift distribution based on our evolving LF model fits.

function fit. This is particularly true for the LF measured using Sérsic magnitudes, which capture a larger fraction of the total light for de Vaucouleurs profile galaxies which dominate the bright end of the LF (e.g. Bernardi et al. 2013). A bright-end excess above a best-fitting Schechter function has been observed in many other surveys (e.g. Loveday et al. 1992; Norberg et al. 2002; Montero-Dorta & Prada 2009) and appears to be particularly pronounced in bluer bands (e.g. Montero-Dorta & Prada 2009; Loveday et al. 2012; Driver et al. 2013). As Driver et al. (2013) point out, given the approximately Gaussian distribution of galaxy colours, the LF cannot be well fitted by a Schechter function in all bands. One should however be aware of the possibility that Sérsic magnitudes, extrapolated as they are out to 10 effective radii, are susceptible to over (or under)estimating the flux of even isolated galaxies if the Sérsic parameters are poorly fit (although the fitting pipeline does attempt to trap for poor fits). Hence, we also show LFs using more stable Petrosian magnitudes.

Our Schechter fits to these LFs are consistent with the r -band LFs determined from the GAMA-I sample by Loveday et al. (2012), using slightly different methods, and shown in Fig. 8 as dotted lines. We also show the ‘corrected’ LF from the Blanton et al. (2005) low-redshift SDSS sample (without colour selection). Considering that this plot is comparing the LFs of SDSS galaxies within only $150 h^{-1}$ Mpc with GAMA galaxies out to $z \approx 0.65$, the agreement is remarkably good, and provides further evidence that the

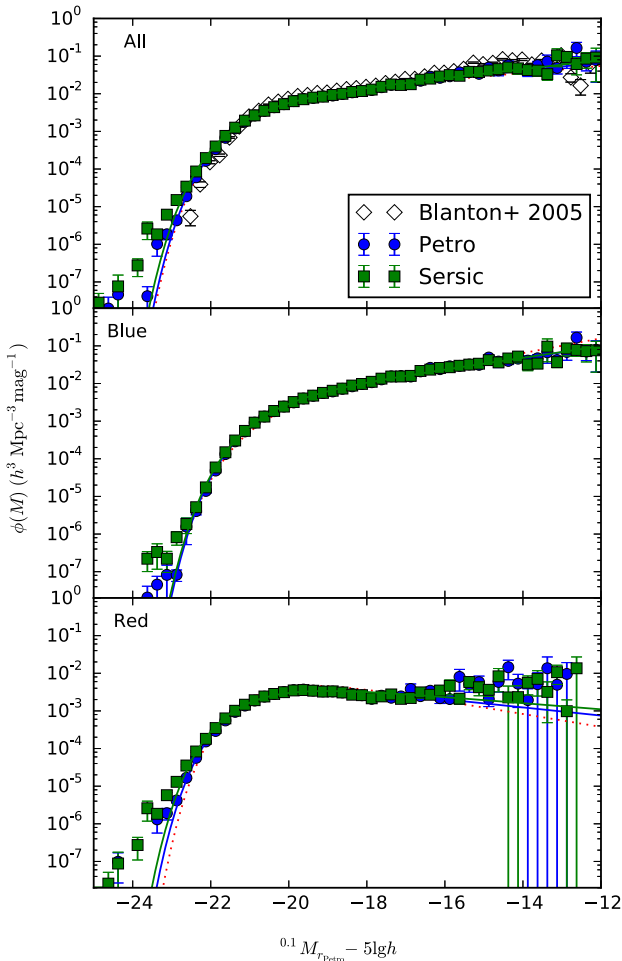


Figure 8. GAMA-II evolution- and density-corrected Petrosian (blue circles) and Sérsic (green squares) r -band LFs with best-fitting Schechter functions (solid lines) assuming evolution parameters for each sample as given in the lower half of Table 3. The dotted lines show the best-fitting r -band Schechter functions from table 5 of Loveday et al. (2012). The open diamonds in the top panel show the ‘corrected’ LF from fig. 7 of Blanton et al. (2005).

simple evolutionary model adopted allows one to accurately recover the evolution-corrected LF, despite its poor performance beyond redshift $z \approx 0.5$ (Fig. 6).

7.4 Testing the evolution model

In Fig. 9, we investigate how faithfully our simple evolution model, namely one in which log-luminosity and log-density evolve linearly with redshift, is able to match the GAMA LF measured in redshift slices. The top panel shows Petrosian r -band LFs for the full GAMA-II sample measured in four redshift slices as indicated, calculated using equation (10) with the best-fitting evolution parameters and radial overdensities, and taking into account the appropriate redshift limits. If the evolution model accurately reflects true evolution, and if we have successfully corrected for density variations, then these LFs should be consistent where they overlap in luminosity. In the bottom panel, we have divided each LF by the LF determined from the full sample ($0.002 < z < 0.65$; top panel of Fig. 8) in order to make differences more clearly visible. We see that the lowest redshift LF, $z < 0.1$, is about 10–20 per cent lower than the $0.1 < z < 0.2$ LF, indicating that the linear

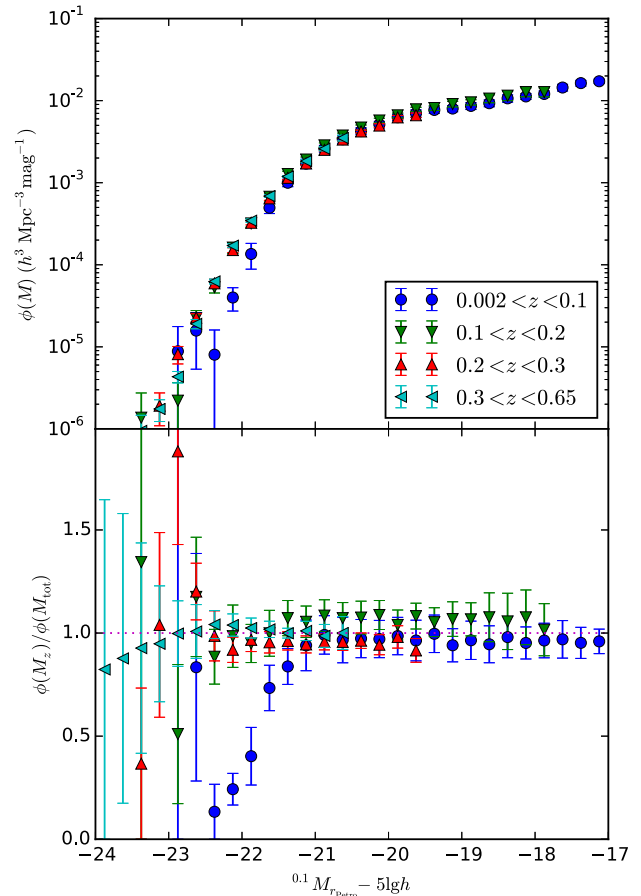


Figure 9. Top panel: Petrosian r -band LFs measured in redshift slices as indicated for the full GAMA sample, applying evolutionary corrections as given in Table 3. Bottom panel: the same LFs relative to the overall LF from the top panel of Fig. 8.

evolution model is somewhat undercorrecting at the lowest redshifts. The low-redshift underdensity is particularly severe at the bright end: the most luminous ($M_r - 5\log h \lesssim -21.5$ mag) galaxies are underdense by ~ 50 per cent relative to the higher redshift slices.

In order to investigate these discrepancies further, we repeat this analysis using redshift-sliced LFs determined using Sérsic magnitudes, with results shown in Fig. 10. The underdensity of luminous, low-redshift galaxies is now much less severe; instead we see an increased scatter between redshifts at the bright end, with perhaps the $0.1 < z < 0.2$ LF biased high relative to the others. It thus seems likely that the underdensity of luminous, low-redshift galaxies apparent in Fig. 9 is largely due to Petrosian magnitudes missing a significant fraction of the flux of luminous galaxies, which will tend to have a de Vaucouleurs-like profile. This problem is further exacerbated for such galaxies at low redshift, which will have large angular extent, and thus also be susceptible to poor background subtraction: Blanton et al. (2011) show that galaxies of radius ~ 100 arcsec have their magnitudes underestimated by around 1.5 mag in the SDSS DR7 data base. Both Sérsic and Petrosian photometry are subject to overblending or ‘shredding’ of large galaxy images. When running the Sérsic fitting pipeline, Kelvin et al. (2012) aimed towards undershredding, as they were specifically focused on the primary galaxies in systems with close neighbours. However, this does mean that the Sérsic fluxes become susceptible to non-detection of nearby

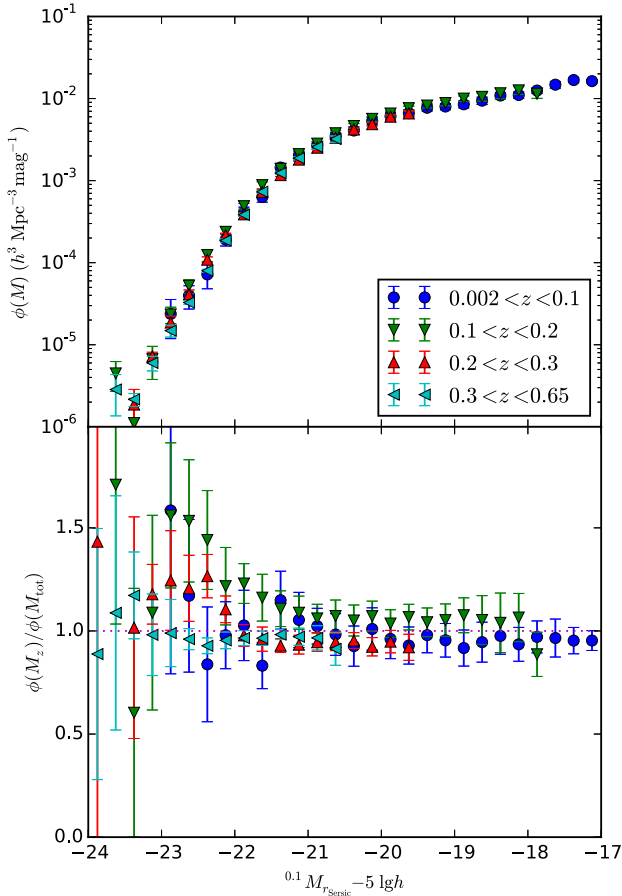


Figure 10. As Fig. 9 but using Sérsic magnitudes.

secondary sources, which introduces a positive flux bias in crowded fields for a small fraction of galaxies, see Section 2.

In conclusion, while the redshift-sliced Petrosian LFs do show some systematic differences, use of GAMA-measured Sérsic magnitudes, which capture a larger fraction of total flux for de Vaucouleurs-profile galaxies, and which have an improved background subtraction compared with SDSS DR7, largely mitigates these differences, and suggests that our evolution model is a reasonable one.

8 DISCUSSION

8.1 Comparison with previous results

While our evolution-corrected LFs agree well with previous estimates, our finding of positive density evolution (in the sense that comoving density was higher in the past) is at odds with most previous work which has tended to find either mildly negative (Cool et al. 2012) or insignificant (Blanton et al. 2003; Moustakas et al. 2013) density evolution. Faber et al. (2007) find a declining comoving number density with redshift for their red sample, with no noticeable density evolution for their blue and full samples. Zucca et al. (2009) also find a declining comoving number density with redshift for their reddest sample; for their bluest galaxies, they find increasing number density with redshift.

At least some of the discrepancy between the sign of the density evolution between us and e.g. Cool et al. (2012) might be explained by the way in which the LF and evolution are fitted. Cool et al.

(2012) fit the characteristic magnitude M^* to each redshift range using the Sandage et al. (1979) maximum-likelihood method, holding the faint-end slope parameter α fixed at its best-fitting value for the lowest redshift range. They then find the normalization ϕ^* using the Davis & Huchra (1982) minimum-variance estimator. Any overestimate of luminosity evolution would lead to a corresponding underestimate in density evolution, due to the assumption of an unchanging faint-end slope with redshift and the strong correlation between Schechter parameters. Although any determination of evolution will be affected by degeneracies between luminosity and density evolution, our method makes no assumption about the (unobserved) faint-end slope of the LF at higher redshifts. On the other hand, we do assume a parametric form for evolution.

It is also plausible that the discrepancies between estimated evolution parameters are due to the uncertainties in incompleteness correction required when analysing most galaxy surveys. For example, when we cap our incompleteness-correction weights to 5, we see a reduction in the estimated density evolution parameters. There are likely to be other effects leading to systematic errors in the determination of evolution parameters, which are not reflected in the (statistical) error contours.

A positive density evolution for the All galaxy sample would suggest a reduction in the number of galaxies with cosmic time, either through merging, or due to galaxies dropping out of the sample selection criteria as they passively fade. Neither scenario seems terribly likely; Robotham et al. (2014) see evidence for only a small merger rate in the GAMA sample. Perhaps a more likely explanation is that the apparent density evolution at low redshift is actually caused by a local underdensity, e.g. Keenan, Barger & Cowie (2013) and Whitbourn & Shanks (2014).

8.2 Future work

There are several ways in which the present work can be extended.

Having derived density-corrected V_{\max} values for each galaxy, it is then trivial to determine other distribution functions, such as the stellar mass and size functions, and their evolution. By way of a quick example, in Fig. 11 we plot the stellar mass function for

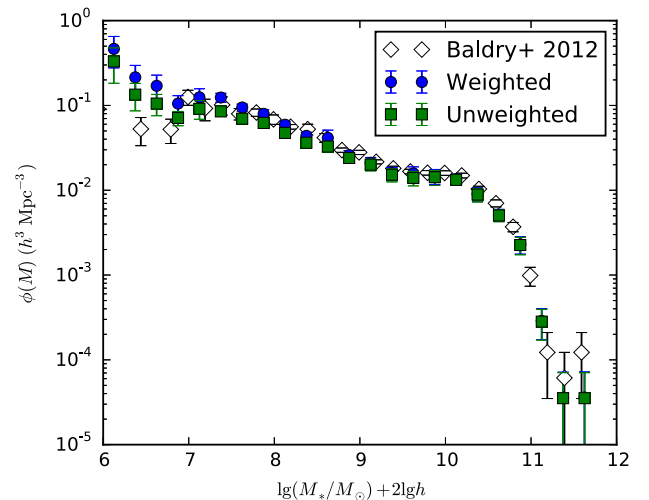


Figure 11. Stellar mass function for low-redshift galaxies ($z < 0.06$) determined from GAMA-II with (blue circles) and without (green squares) applying a weighting correction for surface-brightness and redshift incompleteness. Comparison data points for GAMA-I data from Baldry et al. (2012) are shown as open diamonds.

low-redshift ($z < 0.06$) GAMA-II galaxies, using the stellar mass estimates of Taylor et al. (2011). In the mass regime where surface-brightness completeness is high, $\log(M/M_{\odot}) + 2 \log h \gtrsim 8$, we find excellent agreement with the earlier estimate from Baldry et al. (2012) using a density-defining population. The upturn seen in the mass function below $\log(M/M_{\odot}) + 2 \log h \approx 7$ will be sensitive to the incompleteness corrections applied; confirmation of this feature will need to await the availability of deeper VLT Survey Telescope Kilo-degree Survey (VST KiDS) imaging in the GAMA regions. Future work will explore the evolution of the stellar mass function.

The density-corrected V_{\max} values will also be used to generate the radial distributions of random points required to measure the clustering of flux-limited galaxy samples (Farrow et al., in preparation)

We plan to explore the possibility of using the Taylor et al. (2011) stellar population synthesis model fits to GAMA data to derive luminosity evolution parameters Q_e for individual galaxies. If the models can predict Q_e with sufficient reliability, the degeneracy in fitting for both luminosity and density evolution would be largely eliminated. This would also allow for the fact that galaxies have individual evolutionary histories.

We also plan to incorporate the environmental dependence of the LF into our model. Note that the radial overdensities shown in Fig. 6 are a poor estimate of the density around each galaxy since they are averages over the entire GAMA-II area within each redshift shell. McNaught-Roberts et al. (2014) present estimates of the LF for galaxies in bins of density within $8h^{-1}$ Mpc spheres. We are currently extending density estimation to the full GAMA sample using a variety of density measures (Martindale et al., in preparation).

This main focus of this paper has been to correct the LF and radial density for the effects of evolution, rather than to measure evolution per se. An alternative way of constraining evolution is to measure how the luminosity of galaxies at a fixed space density evolves. Via comparison with a model for the evolution of stellar populations (or luminosity evolution of the Fundamental Plane), one can estimate the rate of mass growth, e.g. Brown et al. (2007).

9 CONCLUSIONS

We have described an implementation of the Cole (2011) JSWML method used to infer the evolutionary parameters, the radial density variations and the r band LF of galaxies in the GAMA-II survey. For the overall population, we find that galaxies have faded in r -band luminosity by about 0.5 mag, and have decreased in comoving number density by a factor of about 1.6 since $z \approx 0.5$, i.e. over the last 5 Gyr or so. When the population is divided into red and blue galaxies, the differences in density evolution parameter P_e are statistically insignificant. Luminosity evolution is significantly stronger for blue galaxies than for red. Evolution in the luminosity density evolution of blue galaxies is higher than that of red at the $\sim 5\sigma$ level. These findings are consistent with those of Loveday et al. (2012) based on GAMA-I and are as expected, since a fraction of galaxies that were blue in the past will have since ceased star formation and become red.

While there still exists some degeneracy between the parameters describing luminosity (Q_e) and density (P_e) evolution for GAMA-II data, see Fig. 5, analysis of simulated data and comparison with a local galaxy sample from SDSS (Blanton et al. 2005) shows that we are able to recover the evolution-corrected LF to high accuracy. In detail, GAMA LFs are poorly described by Schechter functions,

due to excess number density at both faint and bright luminosities, particularly for the red population.

The density-corrected V_{\max} values will be made available via the GAMA data base (<http://www.gama-survey.org/>).

ACKNOWLEDGEMENTS

JL acknowledges support from the Science and Technology Facilities Council (grant number ST/I000976/1) and illuminating discussions with Shaun Cole. PN acknowledges the support of the Royal Society through the award of a University Research Fellowship, the European Research Council, through receipt of a Starting Grant (DEGAS-259586) and the Science and Technology Facilities Council (ST/L00075X/1). It is also a pleasure to thank the referee, Thomas Jarrett, for his careful reading of the paper and for his many useful suggestions.

GAMA is a joint European-Australasian project based around a spectroscopic campaign using the Anglo-Australian Telescope. The GAMA input catalogue is based on data taken from the Sloan Digital Sky Survey and the UKIRT Infrared Deep Sky Survey. Complementary imaging of the GAMA regions is being obtained by a number of independent survey programmes including GALEX MIS, VST KiDS, VISTA VIKING, WISE, Herschel-ATLAS, GMRT and ASKAP providing UV to radio coverage. GAMA is funded by the STFC (UK), the ARC (Australia), the AAO, and the participating institutions. The GAMA website is: <http://www.gama-survey.org/>.

REFERENCES

- Abazajian et al., 2009, ApJS, 182, 543
 Baldry I. K., Glazebrook K., Brinkmann J., Ivezić v., Lupton R. H., Nichol R. C., Szalay A. S., 2004, ApJ, 600, 681
 Baldry I. K., Balogh M. L., Bower R. G., Glazebrook K., Nichol R. C., Bamford S. P., Budavari T., 2006, MNRAS, 373, 469
 Baldry I. K. et al., 2010, MNRAS, 404, 86
 Baldry I. K. et al., 2012, MNRAS, 421, 621
 Baldry I. K. et al., 2014, MNRAS, 441, 2440
 Bell E. F., McIntosh D. H., Katz N., Weinberg M. D., 2003, ApJS, 149, 289
 Benson A., Bower R., Frenk C., Lacey C., Baugh C., Cole S., 2003, ApJ, 599, 38
 Bernardi M., Meert A., Sheth R. K., Vikram V., Huertas-Company M., Mei S., Shankar F., 2013, MNRAS, 436, 697
 Bertin E., Arnouts S., 1996, A&AS, 117, 393
 Blanton M. R., Roweis S., 2007, AJ, 133, 734
 Blanton M. R. et al., 2001, AJ, 121, 2358
 Blanton M. R. et al., 2003, AJ, 125, 2348
 Blanton M. R., Lupton R. H., Schlegel D. J., Strauss M. A., Brinkmann J., Fukugita M., Loveday J., 2005, ApJ, 631, 208
 Blanton M. R., Kazin E., Muna D., Weaver B. A., Price-Whelan A., 2011, AJ, 142, 31
 Brown M. J. I., Dey A., Jannuzi B. T., Brand K., Benson A. J., Brodwin M., Croton D. J., Eisenhardt P. R., 2007, ApJ, 654, 858
 Cole S., 2011, MNRAS, 416, 739
 Cool R. J. et al., 2012, ApJ, 748, 10
 Davis M., Huchra J., 1982, ApJ, 254, 437
 Driver S. P. et al., 2011, MNRAS, 413, 971
 Driver S. P. et al., 2013, MNRAS, 427, 3244
 Efsthathiou G., Ellis R. S., Peterson B. A., 1988, MNRAS, 232, 431
 Ellis S. C., Bland-Hawthorn J., 2007, MNRAS, 377, 815
 Faber S. M. et al., 2007, ApJ, 665, 265
 Hill D. T. et al., 2011, MNRAS, 412, 765
 Keenan R. C., Barger A. J., Cowie L. L., 2013, ApJ, 775, 62
 Kelvin L. S. et al., 2012, MNRAS, 421, 1007
 Kelvin L. S. et al., 2014a, MNRAS, 439, 1245
 Kelvin L. S. et al., 2014b, MNRAS, 444, 1647

- Lin H., Yee H. K. C., Carlberg R. G., Morris S. L., Sawicki M., Patton D. R., Wirth G., Shepherd C. W., 1999, *ApJ*, 518, 533
- Loveday J., Peterson B. A., Efstathiou G., Maddox S. J., 1992, *ApJ*, 390, 338
- Loveday J. et al., 2012, *MNRAS*, 420, 1239
- McNaught-Roberts T. et al., 2014, *MNRAS*, 445, 2125
- Montero-Dorta A. D., Prada F., 2009, *MNRAS*, 399, 1106
- Moustakas J. et al., 2013, *ApJ*, 767, 50
- Norberg P. et al., 2002, *MNRAS*, 336, 907
- Peebles P. J. E., 1980, *The large-scale Structure of the Universe*. Princeton Univ. Press, Princeton, NJ
- Peng Y.-j. et al., 2010, *ApJ*, 721, 193
- Petrosian V., 1976, *ApJ*, 209, L1
- Robotham A. S. G. et al., 2014, *MNRAS*, 444, 3986
- Sandage A., Tammann G. A., Yahil A., 1979, *ApJ*, 232, 352
- Saunders W., Rowan-Robinson M., Lawrence A., Efstathiou G., Kaiser N., Ellis R. S., Frenk C. S., 1990, *MNRAS*, 242, 318
- Schechter P., 1976, *ApJ*, 203, 297
- Schlegel D. J., Finkbeiner D. P., Davis M., 1998, *ApJ*, 500, 525
- Schmidt M., 1968, *ApJ*, 151, 393
- Sérsic J. L., 1963, *Bol. la Asoc. Argentina Astron. La Plata Argentina*, 6, 41
- Stoughton C. et al., 2002, *AJ*, 123, 485
- Taylor E. N. et al., 2011, *MNRAS*, 418, 1587
- Taylor E. N. et al., 2015, *MNRAS*, 446, 2144
- Tonry J. L., Blakeslee J. P., Ajhar E. A., Dressler A., 2000, *ApJ*, 530, 625
- Whitbourn J. R., Shanks T., 2014, *MNRAS*, 437, 2146
- Zucca E. et al., 2009, *A&A*, 508, 1217

This paper has been typeset from a $\text{\TeX}/\text{\LaTeX}$ file prepared by the author.